

## Highly Stretchable, Soft, Low-Hysteresis, and Self-Healable Ionic Conductive Elastomers Enabled by Long, Functional Cross-Linkers

Yufei Wang, Xiaohui Yu, Haopeng Zhang, Xiaoshan Fan,\* Yiting Zhang, Zibiao Li, Yue-E Miao, Xu Zhang,\* and Tianxi Liu\*



Cite This: *Macromolecules* 2022, 55, 7845–7855



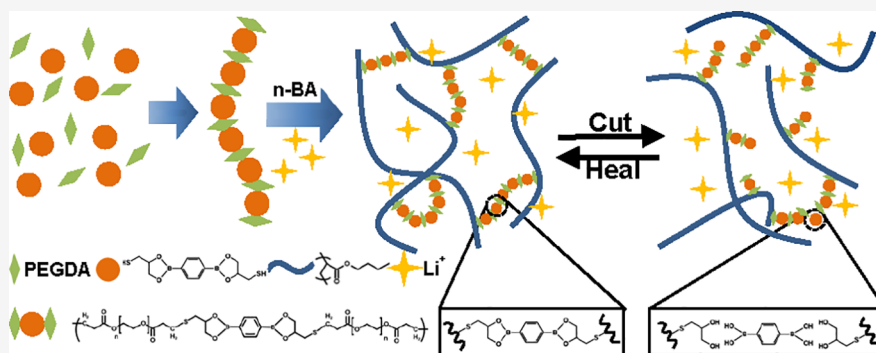
Read Online

ACCESS |

Metrics & More

Article Recommendations

Supporting Information



**ABSTRACT:** Herein, a novel strategy has been developed for the preparation of high-performance conductive elastomers featuring long functional polymer cross-linkers. The macromolecular cross-linkers containing multi boronic ester bonds in the backbone were designed via thiol/acrylate reactions between poly(ethylene glycol) diacrylate (PEGDA) and a dithiol-containing boronic ester (BDB). The obtained PEG–BDB was copolymerized with *n*-butyl acrylate (*n*-BA) to provide PBA/PEG–BDB elastomers. The resultant elastomers exhibit combined desirable properties of high stretchability, low Young’s modulus, low hysteresis, and self-healing performance, simultaneously. To demonstrate their practical applications, sensors based on PBA/PEG–BDB were successfully attached onto diverse joints (wrist, elbow, and finger) of the puppet for real-time motion detection. What is more, the elastomer sensors could well recognize other human activities like writing. This work offers a new design strategy for flexible sensors by optimizing the cross-linked dimension with long functional polymer chains as cross-linkers.

### 1. INTRODUCTION

Flexible electronics have generated increasing attention in recent years for a broad range of promising applications benefiting from their unique advantages including being lightweight, stretchable, and flexible and having comfortable human–machine interaction experiences.<sup>1–5</sup> Conductive elastomers possessing high extensibility<sup>6–9</sup> and recoverable capability<sup>10–12</sup> can act as ideal stretchable electrodes in capacitive or resistive sensors<sup>13–16</sup> and have pushed for rapid growth in the related field of flexible electronics.<sup>17–19</sup> In practical applications, conductive elastomers will inevitably suffer from mechanical damage upon scratch or rupture, thus shortening the elastomers’ service life and reducing their durability. Inspired by biological systems which can spontaneously self-repair,<sup>20–23</sup> the fabrication of self-healing materials mimicking nature’s ability has accomplished rapid advances in recent years.<sup>24,25</sup> For those self-healing materials, they are capable of restoring their original mechanical properties and functionality upon damage, thereby significantly prolonging the materials’ life spans and enhancing their reliability.<sup>26,27</sup> Therefore, it is highly desirable for conductive elastomers to

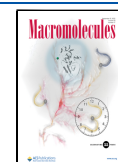
have the interesting self-healing ability that allows for damage repair.<sup>28,29</sup>

To impart self-healing capability to the elastomers, elegant dynamic bonds (dynamic chemical and physical bonds) must be introduced into the polymer network.<sup>30–34</sup> The incorporation of dynamic bonds provides the elastomers with self-healing capability, which could be induced via the reversible breaking and reformation of these bonds. As compared, the reversible chemical bonds such as disulfide,<sup>35–37</sup> imine,<sup>38–41</sup> and boronic ester bonds,<sup>9,41–43</sup> which combine the merits of both normal chemical and dynamical physical bonds, are particularly promising for the fabrication of self-healing elastomers due to their strong, stable yet dynamic nature. The covalently cross-linked elastomers exhibit excellent

**Received:** March 21, 2022

**Revised:** August 23, 2022

**Published:** August 30, 2022



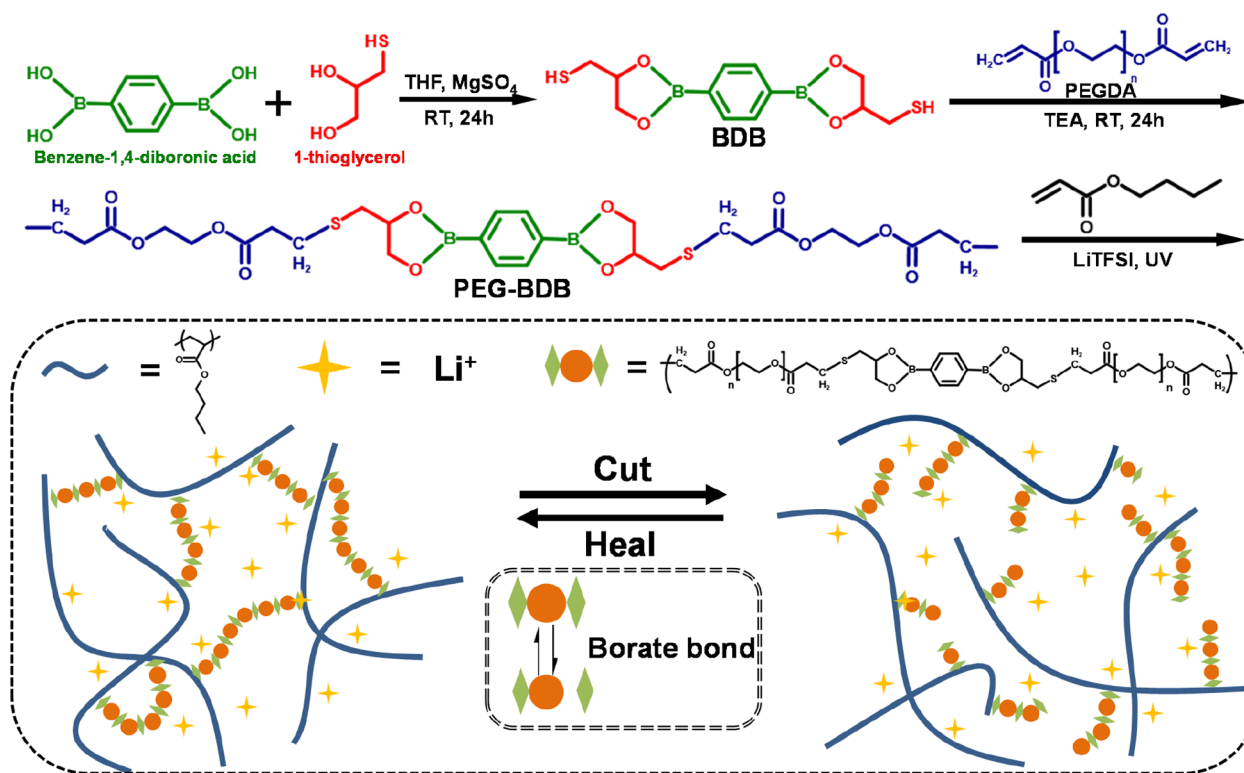


**Figure 1.** Schematic illustration of the synthetic route and dynamic interactions involved in the network construction of the PBA/PEG–BDB ionic conductive elastomers.

mechanical properties deriving from the high strength bonds.<sup>44</sup> However, these elastomers are generally fabricated by employing small reversible molecules as cross-linkages,<sup>43,45,46</sup> and the high density of cross-linkers makes the materials stiffer,<sup>47</sup> which may lead to uncomfortable human–machine experiences.<sup>48,49</sup> Meanwhile, the elevated temperature is usually required for fulfilling self-healing due to reduced chain mobility.<sup>50,51</sup> In addition, these densely cross-linked elastomers usually exhibit lower stretchability, and significant hysteresis is often observed due to the rupturing and rearrangement of dynamic bonds under large deformation.<sup>52</sup> These intrinsic features of conventional self-healing elastomers cannot well meet the requirements of softness, high stretchability, easy control self-healing processes, and fatigue resistance for flexible wearable sensors. In general, it is still a huge challenge to fabricate high-performance elastomers simultaneously possessing the combined good properties mentioned above.<sup>53–55</sup>

To acquire the elastomers with the above-mentioned good properties, the density of cross-linkers must be lowered. For conventional elastomers, this requirement is impossible to meet without the sacrifice of self-healing efficiency. Herein, we developed a novel, simple yet efficient approach to fabricate high-performance elastomers, which feature special long polymer chains containing multi-dynamic motifs as cross-links, as depicted in Figure 1. As compared, the flexible long-chain structure of the macromolecular cross-linkers could significantly improve the motion of polymer chains in the network. In addition, the transesterification reaction between boronic ester bonds on the macromolecular cross-linkers will also help to increase the polymer chain mobility. Therefore, the formed elastomers display a combination of desirable features such as high stretchability, outstanding elastic

recovery, and satisfactory self-healing efficiency. Moreover, the longer macromolecular cross-linkers containing PEG segments will be helpful to increase the ionic conductivity of the resulting materials. With such advantages, the as-prepared elastomers might be the ideal materials for flexible devices, and the wearable sensors were further fabricated to verify their application.

## 2. EXPERIMENTAL SECTION

**2.1. Materials.** *n*-butylacrylate (97.0%) and poly(ethylene glycol) diacrylate ( $M_n = 600$ ) were obtained from Aladdin Regent Co., Ltd. 1-thioglycerol (99.0%) was purchased from Macklin Biochemical Co., Ltd. Anhydrous magnesium sulfate (99.0%) was obtained from Sinopharm Chemical Reagent Co., Ltd. 1,4-Phenylenediboric acid (99.0%) was obtained from Bide Pharmatech Ltd. Tetrahydrofuran (THF) (98.0%) and triethylamine were purchased from Adamas. Triethylamine and THF were dried over a solvent drying system. The deuterated solvents for NMR analysis were obtained from Cambridge Isotope Laboratories, Inc. All other reagents were used as received without further purification. All tests were performed at room temperature unless otherwise specified.

**2.2. Synthesis of 2,2'-(1,4-Phenylene)-bis[4-mercaptan-1,3,2-dioxaborolane].** The preliminary cross-linker, a dithiol-containing boronic ester, was synthesized from the complexation between benzene-1,4-diboric acid and 1-thioglycerol. In brief, benzene-1,4-diboric acid (4.01 g, 24.10 mmol) and 1-thioglycerol (6.52 g, 60.25 mmol) were added to a round-bottom flask containing 100 mL of THF and stirred at room temperature for 1 h until complete dissolution of all compounds. And then,  $MgSO_4$  (7.51 g) was added into the flask. After stirring at room temperature for 24 h, the solution was filtered and concentrated under reduced pressure. Then, the obtained solid was purified by washing five times with 250 mL of heptane. Finally, the purified dithiol dioxaborolane (BDB) as a white solid was dried in a vacuum oven at 40 °C (yield: 8.0 g, 91%).

**2.3. Synthesis of PEG–BDB Long Functional Cross-Linkers.** The preliminary cross-linker BDB (2.95 g, 9.50 mmol), poly(ethylene

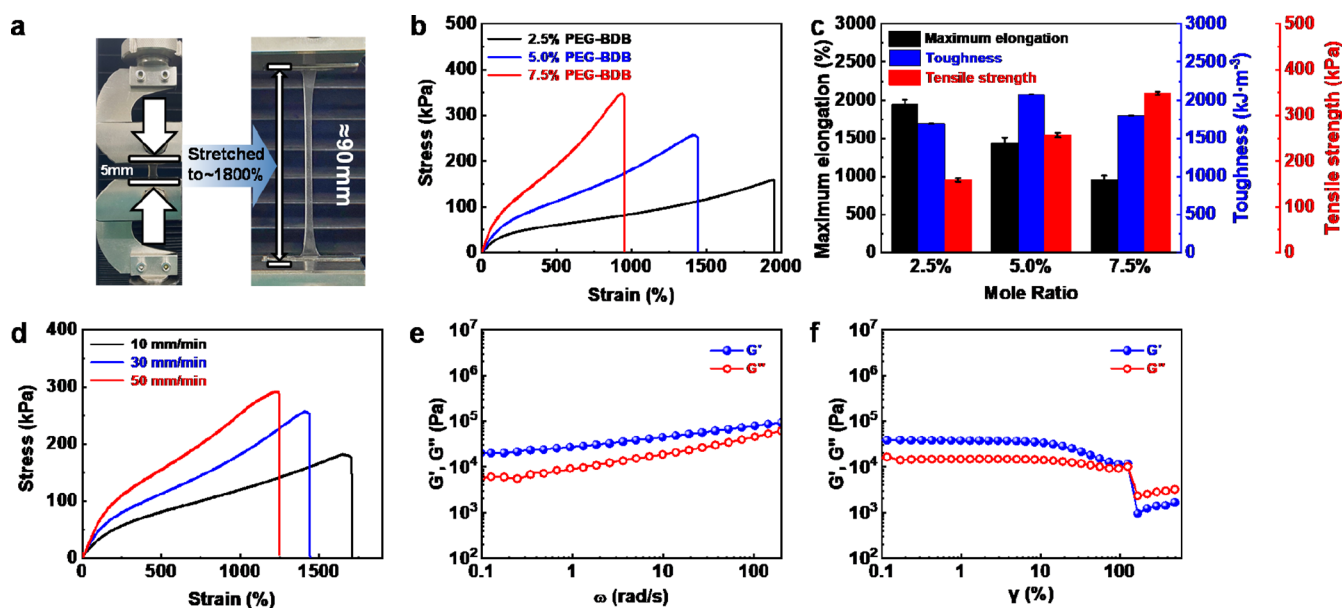


**Figure 2.** (a) Digital photographs of the PBA/PEG-BDB-5% elastomers before and upon stretching. (b) Stress–strain curves and (c) maximum elongation, toughness, and tensile strength of the elastomers with different contents of PEG-BDB cross-linkers. (d) Stress–strain curves of the PBA/PEG-BDB-5% elastomers at different tensile speeds. (e) Frequency dependencies of  $G'$  and  $G''$  of the elastomers. (f) Strain sweep measurements of the elastomer from 0.1 to 500%.

glycol) diacrylate ( $M_n = 600$ ) (6.00 g, 0.01 mol), and triethylamine (0.10 g) were added into a round-bottom flask containing 10 mL of THF and stirred at room temperature for 24 h under a nitrogen atmosphere. Then, the mixture was filtered and concentrated under reduced pressure. The crude product PEG-BDB was further purified by adding dropwise to the cold diethyl ether at 0 °C under stirring. The mixture was then left to stir for 30 min. By centrifugation, the targeted long functional cross-linker was finally obtained as a yellowish viscous liquid and stored at 3 °C in the nitrogen atmosphere (yield: 8.6 g, 96%).

Two long cross-linkers with different polymer chain lengths were prepared by varying the molar ratio of monomers PEGDA to BDB. They are denoted as PEG-BDB-(1:1) and PEG-BDB-(2:1), respectively, in which 1:1 and 2:1 stand for the molar ratio of PEGDA to BDB. (PEG-BDB-(1:1):  $M_n = 5120$  kg/mol, PDI = 1.33; PEG-BDB-(2:1):  $M_n = 1680$  kg/mol, PDI = 1.28).

**2.4. Preparation of PBA/PEG-BDB Ionic Conductive Elastomers.** Elastomers were prepared by copolymerization of *n*-butylacrylate (BA) and the PEG-BDB monomer with different feed ratios in the presence of lithium salts, which are abbreviated as PBA/ $x$  %-PEG-BDB, where  $x$  % refers to the content of the PEG-BDB macromolecular cross-linker in the mixture of PEG-BDB and *n*-BA. As an example, the elastomer PBA/PEG-BDB-5% (BA/PEG-BDB monomer = 19:1) was synthesized as follows: the PEG-BDB monomer (0.05 g) was first uniformly dispersed in the *n*-butylacrylate (0.95 g), and then the bis(trifluoromethane) sulfonimide lithium salts (LiTFSI) (0.40 g) were added into the mixture. After all compounds were dissolved completely, the initiator (BAPO) (0.01 mg) was added. After removing oxygen via purging nitrogen for 30 min, the mixture was uniformly poured into a polytetrafluoroethylene mold. The elastomers were obtained by photo-initiating polymerization in an ultraviolet box for 1 h. All prepared ionic conductive elastomers had a thickness of around 1 mm.

**2.5. Characterizations.** The  $^1\text{H}$  NMR spectra of BDB and PEG-BDB were recorded on an Avance III 600MHz NMR spectrometer using  $\text{CDCl}_3$  as the solvent. The rheological behaviors of the P(BA/PEG-BDB) samples were measured using a HAAKE MARS rheometer using a 25 mm parallel plate geometry and investigated at an angular frequency ( $\omega$ ) ranging from 1 to 100  $\text{rad s}^{-1}$  at a fixed oscillatory strain of 1%. The temperature-dependent rheological behaviors were measured from 5 to 100 °C at a heating-cooling rate

of 10 °C  $\text{min}^{-1}$  at an angular frequency and a fixed oscillatory strain of 10  $\text{rad s}^{-1}$  and 1%, respectively. The dynamic mechanical behaviors of the PBA/PEG-BDB samples at different temperatures were measured at an angular frequency ranging from 1 to 100  $\text{rad s}^{-1}$  at a fixed oscillatory strain of 1%. The apparent activation energy ( $E_a$ ) for the flow of PBA/PEG-BDB samples was estimated by using the Arrhenius equation,  $\alpha = A e^{E_a/RT}$ , where  $\alpha$  is the shift factor,  $A$  is a constant, and  $R$  is the ideal gas constant. The alternate step-strain sweeps of the PBA/PEG-BDB samples were performed by alternating 1 and 200% shear strains four times at a fixed frequency of 10  $\text{rad s}^{-1}$ . The tensile tests of the PBA/PEG-BDB samples ( $10 \times 5 \times 2$  mm) were performed on a universal testing machine (SANS, Shenzhen, China) and recorded at a tensile rate of 20  $\text{mm min}^{-1}$ . All the tensile measurements were tested at room temperature, and the samples were placed in a humidity chamber (30 °C, RH: 80%) for 12 h before the tests. For qualitatively demonstrating the self-healing performance, the PBA/PEG-BDB samples were cut into two pieces and made to come into contact with each other with a tiny force for 30 min. The optical microscopy images and movies of the fractured and healed PBA/PEG-BDB samples were evaluated using an optical microscope at 25 °C (BX-51, Olympus). The thermal gravimetric analysis (TGA) was performed on a TG 209 F1 from room temperature to 600 °C in the  $\text{N}_2$  atmosphere with a heating rate of 10 °C  $\text{min}^{-1}$ .

**2.6. Measurements of the PBA/PEG-BDB Resistance Sensors.** The resistive-type strain sensing device was assembled with two copper foil current collectors sandwiched with a PBA/PEG-BDB sample ( $5 \times 1 \times 1$  mm), and the copper foil current collectors were used for connecting the testing wires. The PBA/PEG-BDB-resistive strain sensor was sealed in VHB tape (3M 4905). The resistance from the strain sensor was measured on a Keithley 2616 System source meter at a voltage of 3 V. The sensors were adhered to the finger, knee, and elbow of a puppet to instantaneously detect diagnosis for simulating complex human motions. The elastomers were covered with an insulating film, and then “D”, “H”, and “U” were written on the insulating film with a pen.

### 3. RESULTS AND DISCUSSION

The intrinsic mechanical properties of elastomers rely on the architectural design of the elastomer networks. The underlying design incorporates well-defined longer cross-linkers that could

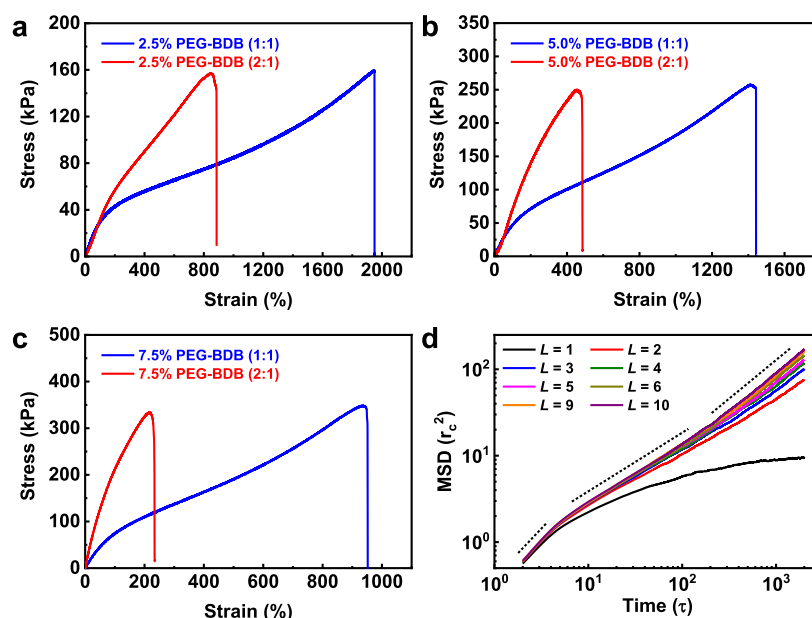


**Figure 3.** Stress–strain curves of PBA/PEG–BDB conductive elastomer films with (a) 2.5%, (b) 5.0%, and (c) 7.5% content of cross-linker contents with different chain lengths. (d) Time dependence of the MSD of polymer chains at different lengths  $L$  of macromolecular cross-linkers.

significantly reduce the cross-linking density and enhance the mobility of the polymer chains. To this end, we designed a loosely cross-linked elastomer using long polymer chains (PEG–BDB) consisting of multi-dynamic boronic esters as cross-linkers. The boronic ester group is known to be a reversible chemical bond, which can be broken and reformed under ambient conditions. It is anticipated that the elaborately designed architecture could bring some interesting properties to the resultant elastomers.

According to the reaction synthesis route shown in Figure 1, the long functional cross-linkers (PEG–BDB) containing multi-dynamic boronic ester bonds in the backbone were obtained. The chemical structures of PEGDA, BDB, and PEG–BDB were verified by the  $^1\text{H}$  NMR technique. As shown in Figure S1b, the signals corresponding to 1-thioglycerol and 1,4-phenylenediboronic acid moieties can be seen clearly, and the integral area ratios of these signals were consistent with the theoretical value, indicating the successful synthesis of BDB. Figure S1c shows the  $^1\text{H}$  NMR spectrum of PEG–BDB, which reveals the existence of characteristic signals belonging to PEGDA and BDB segments. Meanwhile, compared with Figure S1a, the characteristic signal assigned to the terminal vinyl groups of PEG–BDB can be seen clearly, which could chemically bond into polymer chains during the polymerization process. In order to explore the influence of the cross-linker length on the mechanical properties of elastomers, two cross-linkers with different lengths were prepared by controlling the molar ratio of PEGDA to BDB. The obtained two long cross-linkers were characterized by GPC, and both of their traces displayed a monomodal peak and obviously shifted toward the higher molecular region as compared with the monomers BDB and PEG, indicating the successful fabrication of the macromolecular cross-linker, as shown in Figure S2.

Considering the increased chain mobility endowed by the macromolecular cross-linkers (PEG–BDB) in the network, the as-prepared conductive elastomers were expected to exhibit good mechanical properties. Accordingly, Figure 2a provides direct insights that the as-prepared elastomers exhibit great

stretchability (elongation of about 1800%) because of the lower cross-linking density structure, much higher than that of the reported BA-based elastomers with small molecular cross-linkers. A series of tests have been performed to systematically investigate the mechanical properties of the as-prepared elastomers. Figure 2b shows the tensile curves of the elastomers with different cross-linker contents. It was obviously observed that the cross-linker content significantly affects the tensile properties of the elastomers. The fracture stress increases from 160 to 349 kPa as the cross-linker content increases from 2.5 to 7.5%, whereas the break strain decreases from 1950 to 950%. Meanwhile, all the samples possess a relatively low elastic modulus, which is attributed to the high flexibility of PBA chains and the reduced cross-linking degree. Therefore, the tensile properties of the elastomers can be controlled by tailoring the cross-linking density. Figure 2c shows the maximum elongation, tensile strength, and toughness of the elastomers with different contents of PEG–BDB. The samples containing 5% PEG–BDB reach the highest toughness; thus, they were selected as optimal samples for the following measurements unless otherwise mentioned. The effect of tensile speed on the mechanical properties of the as-prepared elastomers was also investigated, as shown in Figure 2d. The fracture stress increases, while the break strain decreases gradually as the tensile speed increases. It can be attributed to the fact that when the elastomers are stretched at a higher speed, the cross-linked network has no time for stress dissipation, the molecular chains and segments are difficult to stretch to the maximum length, and the external force required to destroy the cross-linked network becomes larger.

The viscoelastic properties of the PBA/PEG–BDB elastomers were further investigated via dynamic rheological tests. The oscillation frequency sweeps were first conducted under a small shear strain (1%), and it was observed that the storage modulus ( $G'$ ) always exceeds its loss modulus ( $G''$ ) over the entire sweep range and displays a dependence on the angular frequency, implying the elastic nature of the as-prepared elastomers (Figure 2e). The oscillatory amplitude

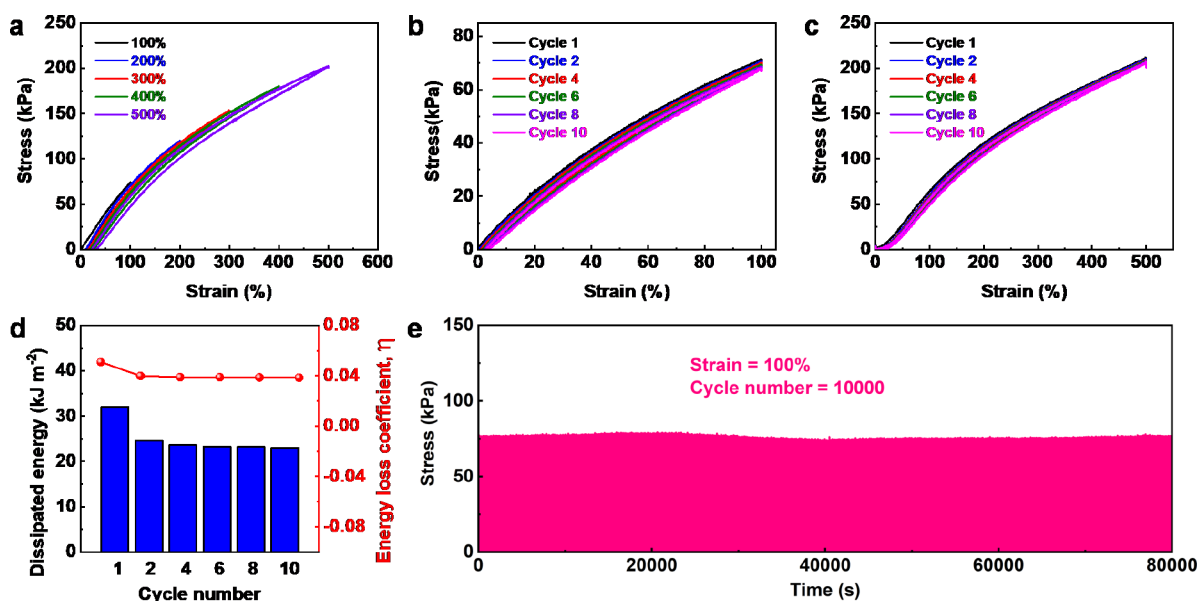


**Figure 4.** (a) Continuous loading–unloading tensile curves of the as-prepared elastomer at different strains. 10 loading–unloading tensile curves at a strain of (b) 100 and (c) 500% without any resting time. (d) Dissipated energy and  $\eta$  at a strain of 500% during 10-cycle loading–unloading tests. (e) Consecutive 10,000 cycles under 100% strain of conductive elastomers.

sweep tests were also performed, as shown in Figure 2f. It can be seen that the  $G'$  of the elastomers is much higher than the  $G''$  at a low shear strain (<100%), indicating the excellent structural integrity of the elastomers. However, the  $G''$  becomes higher than  $G'$  at the relatively larger shear strain (>100%), revealing the translation of the solid-like network structure of the elastomers into the viscous fluid.

In order to investigate the effect of the PEG–BDB cross-linker length on mechanical properties, the elastomers cross-linked by two kinds of macromolecular cross-linkers with different chain lengths were prepared via a similar polymerization process. The tensile stress–strain curves are shown in Figure 3a–c. It can be seen that, as long as the macromolecular cross-linker content is the same, the strain at the break of the elastomers with longer cross-linkers is always higher than that of the shorter cross-linkers. However, the stress at the break of the former is nearly the same as that of the latter. These results further confirmed that the longer spacer in the cross-linked network could improve the flexibility of PBA chains and reduce the degree of cross-linking, thus resulting in the elastomers with high stretchability. Furthermore, the effect of the cross-linker length on mechanical properties could also be attributed to the motion of polymer (PBA) chains. To address this issue, we employed a coarse-grained mesoscopic simulation approach, that is, dissipative particle dynamics (DPD) (see “S2.1 Dissipative Particle Dynamics” and “S2.2 Model and Condition” in the Supporting Information) to study the motion of polymer chains in the macromolecularly cross-linked elastomers. The mobility of polymer chains was quantified by the time dependence of their mean square displacement (MSD) (see “S2.3 Mean Square Displacement” in the Supporting Information), as presented in Figure 3d. It can be seen that the MSD behaviors vary from the short-time linear stage to the sublinear stage and to the long-time linear stage.<sup>56</sup> The MSD curves in the short time almost overlap, indicating the independence of short-time diffusion on the length  $L$  of cross-linkers (identical to the results in Figure 3a–3c). As the time scale increases, the effect of the cross-linker length ( $L$ )

becomes much more significant. Notably, the MSD curves shift upward with increasing the length  $L$  of macromolecular cross-linkers at a relatively longer time scale, implying that the mobility of polymer chains is elevated as the cross-linkers become longer because the longer distance between two adjacent cross-linking junctions (i.e., longer spacers in the cross-linked network) tends to less suppress the motion of polymer chains. It can be concluded from Figure 3d that longer functional cross-linkers make the spacer of the cross-linked network larger, leading to the increase in the elongation at the break with almost unchanged strength as shown in Figure 3a–c.

To examine the energy dissipation mechanism of the PBA/PEG–BDB elastomers, the cyclic stress–strain tests without waiting time between two consecutive loadings were performed with gradually increasing the strains. At different strains ranging from 100 to 500%, elastomers display an inconspicuous hysteresis loop in each cycle (Figure 4a), indicating the excellent resilience of elastomers. The elastomers could almost recover to the original state after each stretching cycle, and the stress corresponding to each deformation cycle is almost the same. The excellent resilience can be attributed to the long-chain cross-linking agent (PEG–BDB) providing long elongation and dynamic covalent bond force in the cross-linked network. To characterize the cyclic stability of the elastomers, 10 uninterrupted cyclic tensile tests with strains of 100 and 500% without any rest time between each cycle were further performed. It was proved that no matter whether under a small strain (100%) or a large strain (500%), the hysteric loop of each cycle of conductive elastomers basically coincides with the first cycle (Figure 4b,c). As shown in Figure 4d, the dissipated energy and energy loss coefficient ( $\eta$ ) were obtained by calculating the area of 500% cyclic hysteresis curves. It can be seen that the elastomers display very low hysteresis and excellent resilience. Except for the first cycle, each cycle remains relatively stable and has low dissipated energy and  $\eta$ . The reason why the dissipated energy and  $\eta$  of the first cycle are higher than that of the other cycles is

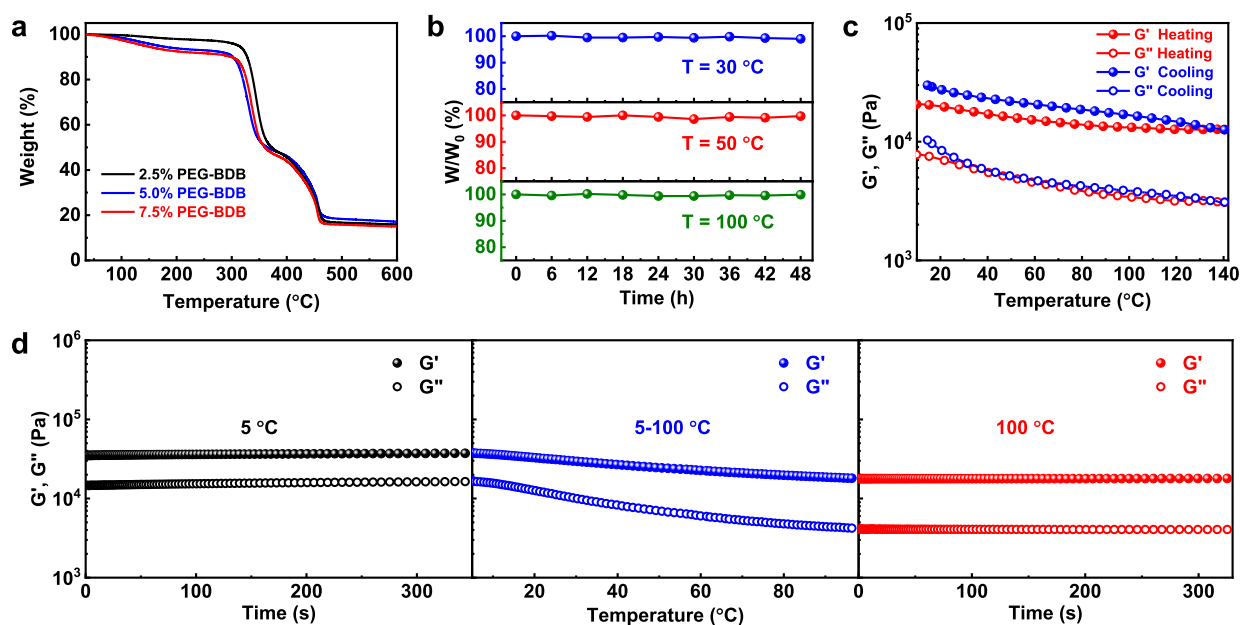


**Figure 5.** (a) TGA curves of the elastomers with different contents of macromolecular cross-linkers (PEG-BDB). (b) Stability testing of the weight of conductive elastomers at different temperatures of 30, 50, and 100 °C. (c) Temperature dependence of  $G'$  and  $G''$  for the elastomers from 10 to 140 °C. (d) Storage modulus  $G'$  and loss modulus  $G''$  of conductive elastomers at 5 °C (left), 5 to 100 °C (middle), and 100 °C (right) with constant frequency.

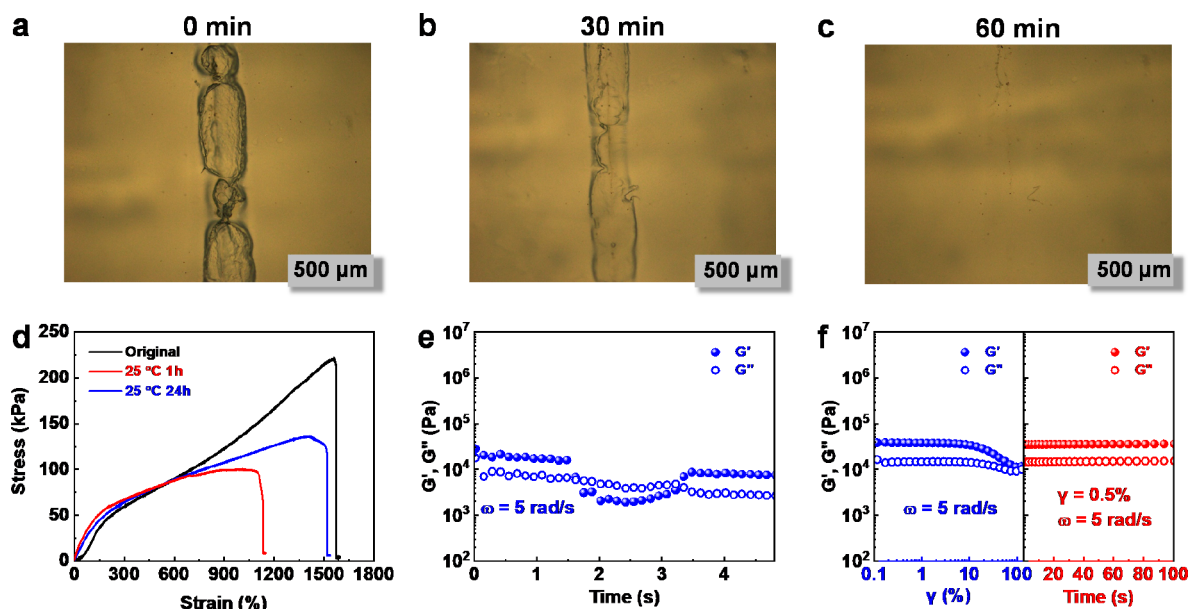


**Figure 6.** (a–c) Time-dependent optical micrographs displaying the self-healing process of the elastomer PBA/PEG-BDB at room temperature. (d) Tensile curves of the original and healed (healing for 1 and 24 h at 25 °C) elastomers. (e) Continuous step-strain sweep with an alternating oscillatory of 1 and 200% at an angular frequency of 5 rad/s. (f) Dynamic strain-time sweep measurements of PBA/PEG-BDB conductive elastomers.

that the cross-linked network is irreversibly damaged when the elastomers are stretched for the first time, and the cross-linked network cannot be fully restored to the initial state after stretching recovery. Afterward, 10,000 continuous cyclic tensile tests at a strain of 100% were performed (Figure 4e). The tensile strength of the elastomers remains almost unchanged during the whole procedure, which proves that the as-prepared conductive elastomers have excellent cycle stability and antifatigue behaviors. As shown in Figure S6, the PBA/PEG-BDB samples have not dissipated the stress for a certain

period of time and still maintain a certain tension at 25 °C. As a comparison, the relaxation time of the sample becomes longer with increasing the PEG-BDB cross-linker content, which further proves that the physical cross-linking as well as the chemical cross-linking formed by the long-chain cross-linker provide a more stable cross-linking network for the elastomer. After 1 h, the stress of the samples is gradually dissipated. This is because boronate bond exchange rearranges the networks in PBA/PEG-BDB. As compared, except for the mechanical strength, the properties of the elastomer with a

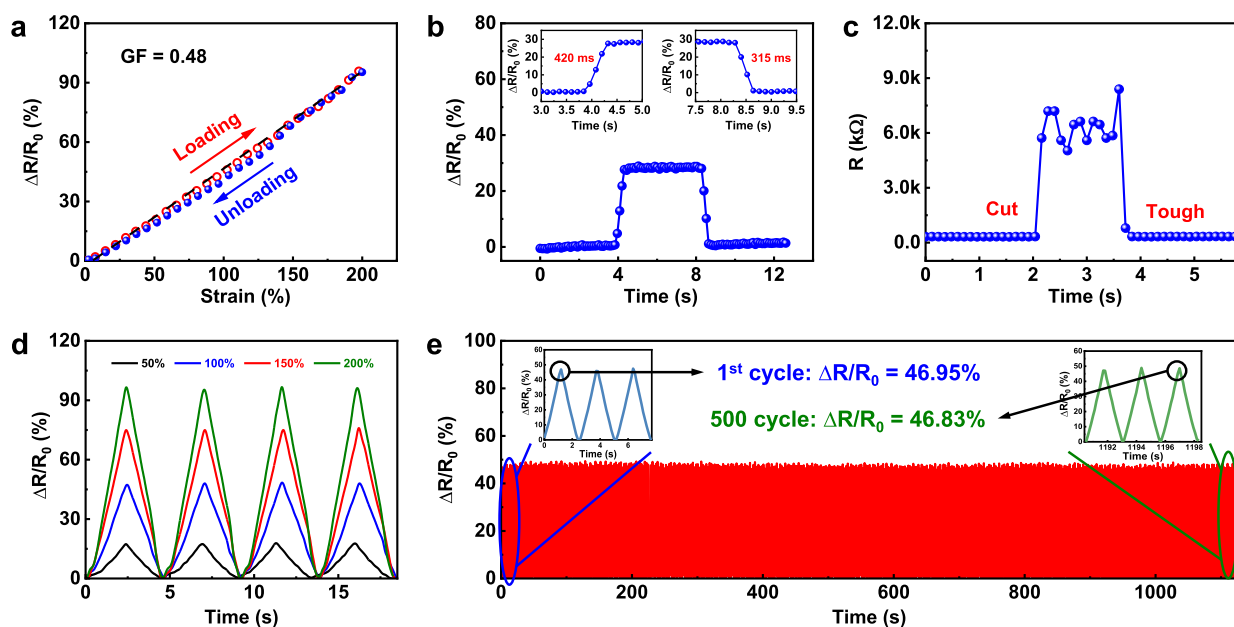


**Figure 7.** Relative resistance variations during (a) loading–unloading cycles and (b) with an instantaneous strain (insets show the response and recovery time). (c) Self-healing ability of electrical signals of the conductive elastomers. (d) Cyclic resistance changes over the strain range of 50–200% at the tensile speed of 50–200 mm min<sup>-1</sup>. (e) 500 compressive cycles at a strain of 100% (insets show the relative resistance of the first cycle and the last cycle).

shorter polymer chain PEG–BDB (2:1) became obviously worse, including elasticity, cycle stability, dissipated energy, and the energy loss coefficient ( $\eta$ ). This is because the higher cross-linking density limits the mobility of the polymer chains and causes the partial breakage of the bonds during the stretching process (Figure S5).

The thermal stability and rheological behavior of the as-prepared elastomers were also investigated. Figure 5a shows the thermogravimetric curves of three PBA/PEG–BDB elastomers differing in the cross-linking degree. It can be observed that the PBA/PEG–BDB elastomers possess a high decomposition temperature up to 300 °C in the N<sub>2</sub> atmosphere, implying that the PBA/PEG–BDB elastomers can possess good stability even under high temperatures. Meanwhile, PBA/PEG–BDB elastomers exhibit excellent stability over a wide range of temperatures under ambient conditions, and the weight furthermore remains unchanged even after being heated at 100 °C for 50 h (Figure 5b). The temperature sweep measurements for the elastomers were presented in Figure 5c, demonstrating that the  $G'$  and  $G''$  gradually decrease with the increase in temperature. The elastomers retain solid-like behaviors, and no sol–gel transition occurs because the storage modulus ( $G'$ ) always remains higher than the loss modulus ( $G''$ ). As shown in Figure 5d, the  $G'$  and  $G''$  of the elastomers remain stable without changing during 300 s at a low temperature (5 °C) and rise up to 100 °C at a constant rate. It can be seen that both  $G'$  and  $G''$  decrease steadily and are instantly stable after the rise in temperature.

Given that the PEG–BDB macromolecular cross-linkers have multi-dynamic boronic bonds in the backbone, the as-prepared elastomers based on PEG–BDB could possess superior self-healing capability, which could be automatically healed after damage by external forces or breakage, consequently prolonging their service life and improving the safety performance. The time-dependent optical micrographs in Figure 6a–c display the self-healing process of the PBA/

PEG–BDB elastomers at room temperature. The elastomers were cut into two slices using a surgical blade, and then they were placed together without extrusion to observe the self-healing process (Figure 6a). It was found that the cracks between two fractured samples gradually decreased after a healing duration of 30 min (Figure 6b) and almost disappeared after a longer time of 60 min (Figure 6c), indicating extremely good self-healing performance. To further investigate the healing efficiency of the PBA/PEG–BDB elastomers, the tensile stress–strain tests of the healed elastomers were performed. As shown in Figure 6d, the recovered fracture strain and tensile strength of the healed elastomers achieve 71.7 and 45.0% of those before cutting after healing for 1 h. As expected, a longer healing time (24 h) could result in the higher recovered fracture strain and tensile strength of 96.0 and 61.5%, respectively, which shows the high healing efficiency. As compared with the fracture strain at the break, the healing efficiency of tensile strength is relatively lower, which may be due to the irreversible fracture of some PBA chains when the elastomers are cut off. The continuous step-strain sweeps with alternate low-amplitude oscillatory (1%) and high-amplitude oscillatory (100%) at 5%  $\omega$  (angular frequency) of the PBA/PEG–BDB elastomers are shown in Figure 6e. Under the low-amplitude oscillatory (1%), the storage modulus ( $G'$ ) is higher than the loss modulus ( $G''$ ). As the high-amplitude oscillatory (100%) is applied to the PBA/PEG–BDB elastomers, the  $G'$  experiences a dramatic drop that becomes lower than the  $G''$ . The  $G'$  and  $G''$  would be rapidly recovered when the oscillatory strain returns to low-amplitude oscillatory (1%), further confirming the high healing efficiency. Moreover, the fast self-repairable behaviors of the PBA/PEG–BDB elastomers could be further confirmed by the dynamic strain-time sweep measurements, as illustrated in Figure 6f. The  $G'$  exceeds  $G''$  in a broad strain range while intersecting with each other as the shear strain increases to about 100%, revealing the rupture of the elastic network. As

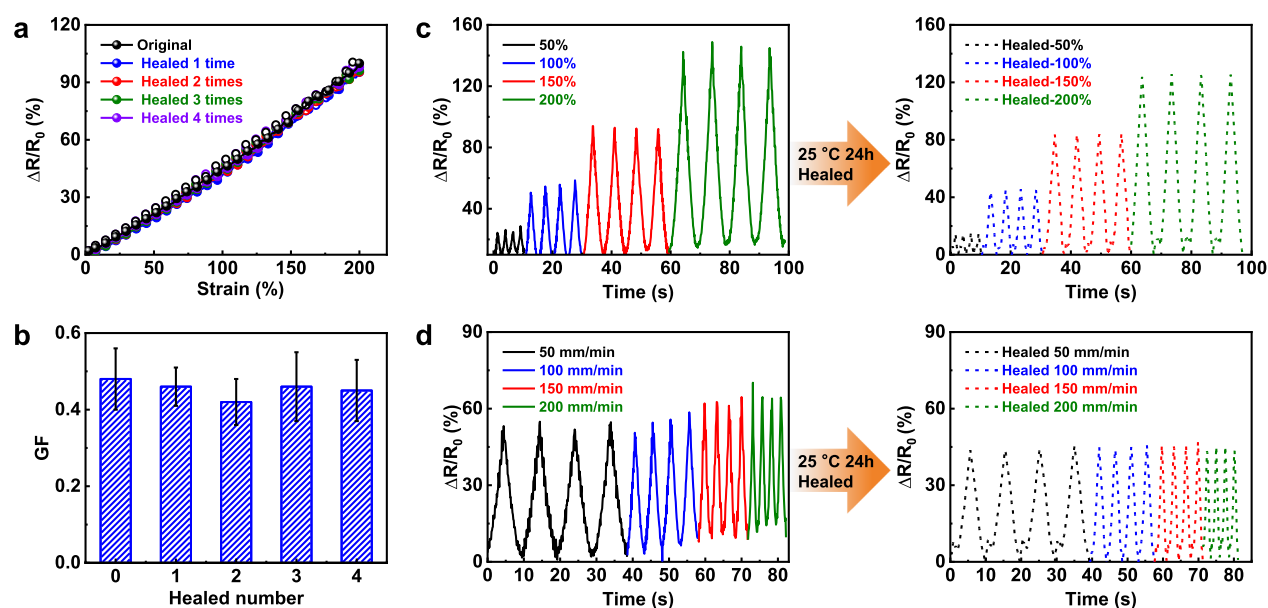


**Figure 8.** (a) Resistance-strain curves and (b) GF of the original sensor and sensors with different healed times (from 1 to 4). Cycle resistance changes of the original and healed (in 24 h at 25 °C) sensors over (c) the strain range of 50–200% at a tensile speed of 100 mm min<sup>-1</sup> and (d) the stretching rate range of 50 to 200 mm min<sup>-1</sup> at a strain of 100%.

the strain is recovered to 0.5%, the  $G'$  and  $G''$  instantly and completely return to their original state, indicating that the elastic network could be immediately self-healed.

These aforementioned results demonstrate that the as-prepared elastomers with an elaborately designed cross-linker PEG–BDB achieved a unique combination of properties including softness, high stretchability, excellent resilience, fatigue resistance, and good self-healing efficiency under ambient conditions. These good properties displayed in the PEG–BDB-based elastomer should be attributed to its unique structure. Especially, few of the reported elastomers in the literature could achieve these good properties simultaneously, as shown in Table S1.<sup>9,57–63</sup>

With the intriguing properties of excellent mechanical properties, good conductivity, high thermal stability, and self-healing capability, the elastomers can be considered as ideal electrodes for future flexible sensor applications. The fabricated sensors could be sensitive to mechanical stimuli including stretching and bending via electronic signals. The sensing performance of the as-fabricated strain sensors was tested under the stretching state. Figure 7a shows that the sensors exhibit a reversible linear relationship between the relative resistance changes versus the applied strains ranging from 0 to 100%, where the gauge factor (GF) value was calculated to be 0.48. As shown in Figure 7b, the response time of the resistance sensors was investigated under 10% tensile strain, and the response and recovery times were calculated to be 420 and 315 ms, respectively, indicating their fast responsive ability. The real-time resistance measurements were further employed to confirm the capability of the self-repairing electrical recovery of conductive elastomers. As shown in Figure 7c, the resistance increases sharply when the elastomers are cut into two pieces; however, it recovers to 99% of the original value in 2 s after the two pieces of elastomers are put together for the self-healing process. Particularly, the sensing performance of the sensors at a high strain (50, 100, 150, and 200%) is both stable and reliable, as shown in Figure 7d. To further study the electrical signal stability and the antifatigue

performance of the as-fabricated sensors, 500 cyclic uninterrupted stress-recovery tests at 100% constant strain were conducted. It can be seen from Figure 7e that the sensors display stable and regular response signals. The  $\Delta R/R_0$  is 46.95 and 46.83% for the first and last cycles, respectively, indicating that the sensors have extremely stable electrical signals. As compared with the reported ionic conductive elastomers, the as-fabricated sensors exhibit excellent electrical signal stability, which is of great significance to the long-term use of the elastomer sensors.

In order to further study the electrical properties after healing, the sensors after being healed for different times (first, second, third, and fourth) were tested by the loading–unloading process under 100% strain. As shown in Figure 8a,b, the GF of the sensors with different healing times is almost the same (first = 0.46, second = 0.42, third = 0.46, and fourth = 0.45) as compared with the original sample, and the loading–unloading lines are well coincided. It was proved that the GF of the sensors remained unchanged after being self-healed several times. The relative resistance changes of the healed elastomers were tested under the strain and stretching rates ranging from 50 to 200% (Figure 8c) and 50 to 200 mm min<sup>-1</sup> (Figure 8d), respectively. As shown in Figure 8c,d, the electrical properties of the sensors based on the healed elastomers are nearly not affected, which means they can still respond regularly to mechanical changes like the original elastomers under the same testing conditions. These results further demonstrated the excellent self-healing ability of the as-prepared elastomers.

To address the practical applications of the conductive elastomers as wearable sensors, a series of relative tests were finally conducted. First, the as-prepared elastomers were connected to the electrical circuits, and the light-emitting diode (LED) bulb could be lighted, as shown in Figure S3. The bulb would become dim during stretching and bright as the external force was removed. This phenomenon indicates that the elastomers possess good conductivity and are sensitive to the variations in strain. Next, the sensors were directly attached onto diverse joints (wrist, elbow, and finger) of the puppet to

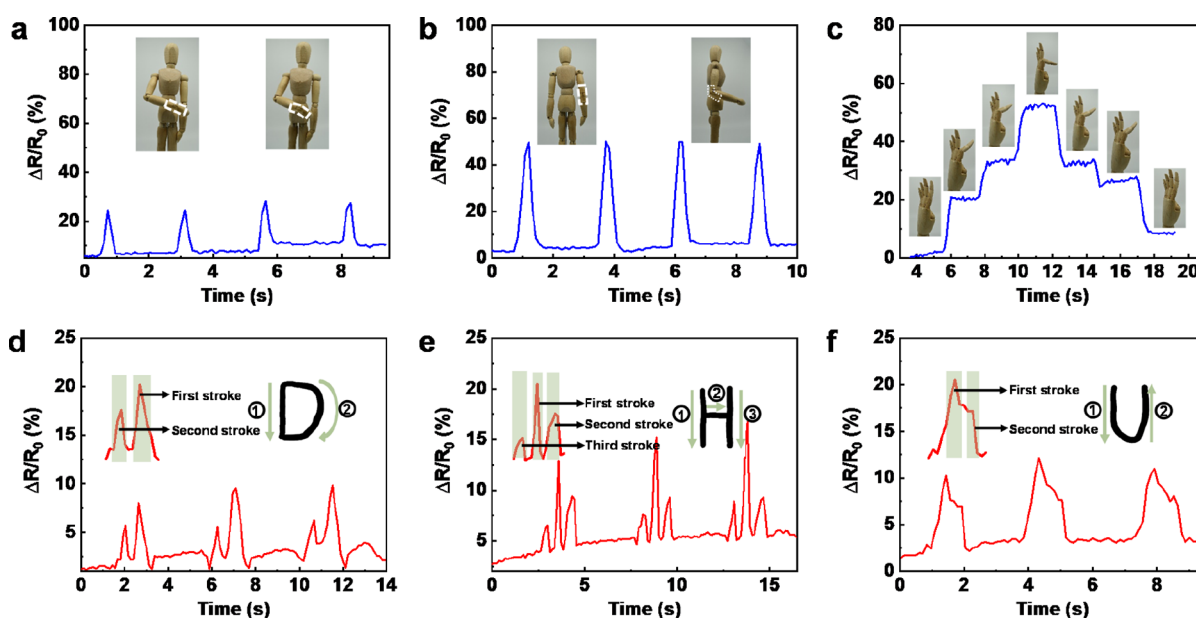


**Figure 9.** Relative resistance variations of the sensor devices fixed on prosthetic (a) wrist-monitoring, (b) elbow-monitoring, and (c) finger-monitoring bending angles. Relative resistance changes of the sensors respond to different deformations by writing (d) “D”, (e) “H”, and (f) “U” on the conductive elastomers.

simulate detecting a wide range of human real-time motions. The apparent relative resistance variations of the elastomers were observed when bending, and the generated electrical signals are highly repeatable and stable, as shown in Figure 9a–c. These desirable strain-dependent sensing properties also allow the elastomer sensors to well recognize other human activities like writing. As displayed in Figure 9d–f, when the capital letters “D” (Figure 9d), “H” (Figure 9e), and “U” (Figure 9f) were written directly with a pen on the sensors, the electrical patterns corresponding to each letter were reproducible; meanwhile, the electrical signals could obviously be distinguished from each other. Overall, the sensors based on PBA/PEG–BDB elastomers have broad prospects in the application fields of wearable flexible sensors for human motion detection thanks to the advantages of excellent mechanical properties, self-healing, and stable and sensitive electrical signals.

#### 4. CONCLUSIONS

In the present study, we developed novel, topologically enhanced chemically cross-linked elastomers containing the long functional polymer chain-bridged PBA. The PEG–BDB polymer chains containing multi-dynamic boronic bonds were primarily formed via thiol/acrylate Michael addition reactions between PEGDA and BDB. As compared with the small molecular agents, the PEG–BDB macromolecular cross-linkers could significantly promote the mobility of polymer chains locked in the cross-linked network. Owing to the optimized cross-linked dimension, the PBA/PEG–BDB elastomers exhibit high stretchability (1950%), low modulus (29 kPa), and negligible hysteresis ( $\eta = 0.039$ ). The relationship between the mechanical properties and the macromolecular cross-linker length was well discussed. Meanwhile, the excellent self-healing ability and reproducible and stable electrical responses were observed in a series of relative tests. When assembled into a flexible sensor, it is capable of precisely detecting human motions (such as wrist, elbow, and finger bending) and other

human activities (such as writing). This study reveals that ionic conductive elastomers featuring long functional macromolecules as cross-linkers are potential candidates for the preparation of high-performance flexible wearable sensors.

#### ■ ASSOCIATED CONTENT

##### Supporting Information

The Supporting Information is available free of charge at <https://pubs.acs.org/doi/10.1021/acs.macromol.2c00563>.

Summary of mechanical, resilience, and self-healing properties of the PBA/PEG–BDB elastomers;  $^1\text{H}$  NMR spectra of the PEG–BDB macromolecular cross-linker and its precursors; GPC traces of PEG–BDB and the monomers; conductivity test photographs of PBA/PEG–BDB elastomers; DPD molecular model and cross-linking process of the functional end beads of the polymer matrix and macromolecular cross-linkers; loading–unloading tensile curves of the PBA/PEG–BDB (2:1) elastomers with 5% PEG–BDB content; and stress-relaxation curves of the PBA/PEG–BDB samples (PDF)

#### ■ AUTHOR INFORMATION

##### Corresponding Authors

**Xiaoshan Fan** – State Key Laboratory for Modification of Chemical Fibers and Polymer Materials, College of Materials Science and Engineering, Donghua University, Shanghai 201620, PR China; [orcid.org/0000-0002-0617-7400](https://orcid.org/0000-0002-0617-7400); Email: [xfan@dhu.edu.cn](mailto:xfan@dhu.edu.cn)

**Xu Zhang** – Key Laboratory of Synthetic and Biological Colloids, Ministry of Education, School of Chemical and Material Engineering, Jiangnan University, Wuxi, Jiangsu 214122, PR China; Email: [xuzhang@jiangnan.edu.cn](mailto:xuzhang@jiangnan.edu.cn)

**Tianxi Liu** – State Key Laboratory for Modification of Chemical Fibers and Polymer Materials, College of Materials Science and Engineering, Donghua University, Shanghai 201620, PR China; Key Laboratory of Synthetic and

Biological Colloids, Ministry of Education, School of Chemical and Material Engineering, Jiangnan University, Wuxi, Jiangsu 214122, PR China; [orcid.org/0000-0002-5592-7386](https://orcid.org/0000-0002-5592-7386); Email: [txliu@jiangnan.edu.cn](mailto:txliu@jiangnan.edu.cn)

## Authors

**Yufei Wang** – State Key Laboratory for Modification of Chemical Fibers and Polymer Materials, College of Materials Science and Engineering, Donghua University, Shanghai 201620, PR China

**Xiaohui Yu** – State Key Laboratory for Modification of Chemical Fibers and Polymer Materials, College of Materials Science and Engineering, Donghua University, Shanghai 201620, PR China

**Haopeng Zhang** – State Key Laboratory for Modification of Chemical Fibers and Polymer Materials, College of Materials Science and Engineering, Donghua University, Shanghai 201620, PR China

**Yiting Zhang** – Key Laboratory of Synthetic and Biological Colloids, Ministry of Education, School of Chemical and Material Engineering, Jiangnan University, Wuxi, Jiangsu 214122, PR China

**Zibiao Li** – Institute of Materials Research and Engineering, A\*STAR (Agency for Science, Technology and Research), Singapore 138634, Singapore; [orcid.org/0000-0002-0591-5328](https://orcid.org/0000-0002-0591-5328)

**Yue-E Miao** – State Key Laboratory for Modification of Chemical Fibers and Polymer Materials, College of Materials Science and Engineering, Donghua University, Shanghai 201620, PR China; [orcid.org/0000-0002-3660-029X](https://orcid.org/0000-0002-3660-029X)

Complete contact information is available at:

<https://pubs.acs.org/10.1021/acs.macromol.2c00563>

## Notes

The authors declare no competing financial interest.

## ACKNOWLEDGMENTS

This work was financially supported by the National Natural Science Foundation of China (52103074, 21875033, and 52161135302), the Research Foundation Flanders (G0F2322N), the Natural Science Foundation of Shanghai (21ZR1402800), and the Innovation Program of Shanghai Municipal Education Commission (2021-01-07-00-03-E00108).

## REFERENCES

(1) Liu, Y.; He, K.; Chen, G.; Leow, W. R.; Chen, X. Nature-Inspired Structural Materials for Flexible Electronic Devices. *Chem. Rev.* **2017**, *117*, 12893–12941.

(2) Guo, J.; Yu, Y.; Cai, L.; Wang, Y.; Shi, K.; Shang, L.; Pan, J.; Zhao, Y. Microfluidics for flexible electronics. *Mater. Today* **2021**, *44*, 105–135.

(3) Gao, W.; Ota, H.; Kiriya, D.; Takei, K.; Javey, A. Flexible Electronics toward Wearable Sensing. *Acc. Chem. Res.* **2019**, *52*, 523–533.

(4) Wang, L.; Chen, D.; Jiang, K.; Shen, G. New insights and perspectives into biological materials for flexible electronics. *Chem. Soc. Rev.* **2017**, *46*, 6764–6815.

(5) Keum, K.; Kim, J. W.; Hong, S. Y.; Son, J. G.; Lee, S.-S.; Ha, J. S. Flexible/Stretchable Supercapacitors with Novel Functionality for Wearable Electronics. *Adv. Mater.* **2020**, *32*, 2002180.

(6) Guo, H.; Han, Y.; Zhao, W.; Yang, J.; Zhang, L. Universally autonomous self-healing elastomer with high stretchability. *Nat. Commun.* **2020**, *11*, 2037.

(7) Yu, X.; Wang, Y.; Zhang, H.; Fan, X.; Liu, T. Ultrastretchable and Stable Conductive Elastomer Based on Micro-Ionicgel for Wide-Working-Range Sensors. *ACS Appl. Mater. Interfaces* **2021**, *13*, 53091–53098.

(8) Wang, Y.; Huang, X.; Zhang, X. Ultrarobust, tough and highly stretchable self-healing materials based on cartilage-inspired non-covalent assembly nanostructure. *Nat. Commun.* **2021**, *12*, 1291.

(9) Xu, J.; Wang, H.; Du, X.; Cheng, X.; Du, Z.; Wang, H. Self-healing, anti-freezing and highly stretchable polyurethane ionogel as ionic skin for wireless strain sensing. *Chem. Eng. J.* **2021**, *426*, 130724.

(10) Wang, Y.; Liu, Y.; Plamthottam, R.; Tebyetekerwa, M.; Xu, J.; Zhu, J.; Zhang, C.; Liu, T. Highly Stretchable and Reconfigurable Ionogels with Unprecedented Thermoplasticity and Ultrafast Self-Healability Enabled by Gradient-Responsive Networks. *Macromolecules* **2021**, *54*, 3832–3844.

(11) Guo, Y.; Yang, L.; Zhang, L.; Chen, S.; Sun, L.; Gu, S.; You, Z. A Dynamically Hybrid Cross-linked Elastomer for Room-Temperature Recyclable Flexible Electronic Devices. *Adv. Funct. Mater.* **2021**, *31*, 2106281.

(12) Xin, Y.; Peng, H.; Xu, J.; Zhang, J. Ultrauniform Embedded Liquid Metal in Sulfur Polymers for Recyclable, Conductive, and Self-Healable Materials. *Adv. Funct. Mater.* **2019**, *29*, 1808989.

(13) Bates, C. M.; Chang, A. B.; Momčilović, N.; Jones, S. C.; Grubbs, R. H. ABA Triblock Brush Polymers: Synthesis, Self-Assembly, Conductivity, and Rheological Properties. *Macromolecules* **2015**, *48*, 4967–4973.

(14) Fan, L.; Xie, J.; Zheng, Y.; Wei, D.; Yao, D.; Zhang, J.; Zhang, T. Antibacterial, Self-Adhesive, Recyclable, and Tough Conductive Composite Hydrogels for Ultrasensitive Strain Sensing. *ACS Appl. Mater. Interfaces* **2020**, *12*, 22225–22236.

(15) Wu, Z.; Chen, J.; Boukhvalov, D. W.; Luo, Z.; Zhu, L.; Shi, Y. A new triboelectric nanogenerator with excellent electric breakdown self-healing performance. *Nano Energy* **2021**, *85*, 105990.

(16) Xu, K.; Wang, Y.; Zhang, B.; Zhang, C.; Liu, T. Stretchable and self-healing polyvinyl alcohol/cellulose nanofiber nanocomposite hydrogels for strain sensors with high sensitivity and linearity. *Compos. Commun.* **2021**, *24*, 100677.

(17) Ling, H.; Liu, S.; Zheng, Z.; Yan, F. Organic Flexible Electronics. *Small Methods* **2018**, *2*, 1800070.

(18) Horejs, C.-M. Flexible electronics: Lasting memories are in sight. *Nat. Rev. Mater.* **2018**, *3*, 18002.

(19) Mao, J.; Zhao, C.; Li, Y.; Xiang, D.; Wang, Z. Highly stretchable, self-healing, and strain-sensitive based on double-cross-linked nanocomposite hydrogel. *Compos. Commun.* **2020**, *17*, 22–27.

(20) Zhang, L.; Liang, J.; Jiang, C.; Liu, Z.; Sun, L.; Chen, S.; Xuan, H.; Lei, D.; Guan, Q.; Ye, X.; You, Z. Peptidoglycan-inspired autonomous ultrafast self-healing bio-friendly elastomers for bio-integrated electronics. *Natl. Sci. Rev.* **2021**, *8*, nwa154.

(21) Yang, J.; Zhang, G.; Wang, J.; Hao, Y.; Hao, G.; Xiao, L.; Chen, J.; Zhou, B.; Fu, J.; Jiang, W. Parthenocissus-inspired, strongly adhesive, efficiently self-healing polymers for energetic adhesive applications. *J. Mater. Chem. A* **2021**, *9*, 16076–16085.

(22) Chen, C.; Ying, W. B.; Li, J.; Kong, Z.; Li, F.; Hu, H.; Tian, Y.; Kim, D. H.; Zhang, R.; Zhu, J. A Self-Healing and Ionic Liquid Affiliative Polyurethane toward a Piezo 2 Protein Inspired Ionic Skin. *Adv. Funct. Mater.* **2022**, *32*, 2106341.

(23) Xu, S.; Li, J.; Qiu, H.; Xue, Y.; Yang, J. Repeated self-healing of composite coatings with core-shell fibres. *Compos. Commun.* **2020**, *19*, 220–225.

(24) Jeong, Y. K.; Choi, J. W. Mussel-Inspired Self-Healing Metallopolymers for Silicon Nanoparticle Anodes. *ACS Nano* **2019**, *13*, 8364–8373.

(25) Liu, Y.; Zheng, J.; Zhang, X.; Du, Y.; Li, K.; Yu, G.; Jia, Y.; Zhang, Y. Mussel-inspired and aromatic disulfide-mediated polyurethane with rapid self-healing performance and water-resistance. *J. Colloid Interface Sci.* **2021**, *593*, 105–115.

(26) Yu, X.; Zheng, Y.; Zhang, H.; Wang, Y.; Fan, X.; Liu, T. Fast-Recoverable, Self-Healable, and Adhesive Nanocomposite Hydrogel

Consisting of Hybrid Nanoparticles for Ultrasensitive Strain and Pressure Sensing. *Chem. Mater.* **2021**, *33*, 6146–6157.

(27) Wang, M.; Nudelmann, F.; Matthes, R. R.; Shaver, M. P. Frustrated Lewis Pair Polymers as Responsive Self-Healing Gels. *J. Am. Chem. Soc.* **2017**, *139*, 14232–14236.

(28) Yao, Y.; Xu, Z.; Liu, B.; Xiao, M.; Yang, J.; Liu, W. Multiple H-Bonding Chain Extender-Based Ultradiff Thermoplastic Polyurethanes with Autonomous Self-Healability, Solvent-Free Adhesiveness, and AIE Fluorescence. *Adv. Funct. Mater.* **2021**, *31*, 2006944.

(29) Wang, X.; Zhan, S.; Lu, Z.; Li, J.; Yang, X.; Qiao, Y.; Men, Y.; Sun, J. Healable, Recyclable, and Mechanically Tough Polyurethane Elastomers with Exceptional Damage Tolerance. *Adv. Mater.* **2020**, *32*, 2005759.

(30) Kang, J.; Tok, J. B. H.; Bao, Z. Self-healing soft electronics. *Nat. Electron.* **2019**, *2*, 144–150.

(31) Wang, S.; Urban, M. W. Self-healing polymers. *Nat. Rev. Mater.* **2020**, *5*, 562–583.

(32) Yang, Y.; Urban, M. W. Self-healing polymeric materials. *Chem. Soc. Rev.* **2013**, *42*, 7446–7467.

(33) Gačaniin, J.; Hedrich, J.; Sieste, S.; Glaßer, G.; Lieberwirth, I.; Schilling, C.; Fischer, S.; Barth, H.; Knöll, B.; Synatschke, C. V.; Weil, T. Autonomous Ultrafast Self-Healing Hydrogels by pH-Responsive Functional Nanofiber Gelators as Cell Matrices. *Adv. Mater.* **2019**, *31*, No. e1805044.

(34) Tong, X.; Tian, Z.; Sun, J.; Tung, V.; Kaner, R. B.; Shao, Y. Self-healing flexible/stretchable energy storage devices. *Mater. Today* **2021**, *44*, 78–104.

(35) Tran, V. T.; Mredha, M. T. I.; Na, J. Y.; Seon, J.-K.; Cui, J.; Jeon, I. Multifunctional poly(disulfide) hydrogels with extremely fast self-healing ability and degradability. *Chem. Eng. J.* **2020**, *394*, 124941.

(36) Rao, Q.; Lu, Y.; Song, L.; Hou, Y.; Zhan, X.; Zhang, Q. Highly Efficient Self-Repairing Slippery Liquid-Infused Surface with Promising Anti-Icing and Anti-Fouling Performance. *ACS Appl. Mater. Interfaces* **2021**, *13*, 40032–40041.

(37) Zhou, J.; Liu, H.; Sun, Y.; Wang, C.; Chen, K. Self-Healing Titanium Dioxide Nanoparticles-Graphene/Multi-Branched Polyurethane Hybrid Flexible Film with Multifunctional Properties toward Wearable Electronics. *Adv. Funct. Mater.* **2021**, *31*, 2011133.

(38) Miao, J.-T.; Ge, M.; Peng, S.; Zhong, J.; Li, Y.; Weng, Z.; Wu, L.; Zheng, L. Dynamic Imine Bond-Based Shape Memory Polymers with Permanent Shape Reconfigurability for 4D Printing. *ACS Appl. Mater. Interfaces* **2019**, *11*, 40642–40651.

(39) Deng, K.; Zhou, S.; Xu, Z.; Xiao, M.; Meng, Y. A high ion-conducting, self-healing and nonflammable polymer electrolyte with dynamic imine bonds for dendrite-free lithium metal batteries. *Chem. Eng. J.* **2022**, *428*, 131224.

(40) Bhattacharya, S.; Phatake, R. S.; Nabha Barnea, S.; Zerby, N.; Zhu, J.-J.; Shikler, R.; Lemcoff, N. G.; Jelinek, R. Fluorescent Self-Healing Carbon Dot/Polymer Gels. *ACS Nano* **2019**, *13*, 1433–1442.

(41) Li, Y.; Yang, L.; Zeng, Y.; Wu, Y.; Wei, Y.; Tao, L. Self-Healing Hydrogel with a Double Dynamic Network Comprising Imine and Borate Ester Linkages. *Chem. Mater.* **2019**, *31*, 5576–5583.

(42) Cromwell, O. R.; Chung, J.; Guan, Z. Malleable and Self-Healing Covalent Polymer Networks through Tunable Dynamic Boronic Ester Bonds. *J. Am. Chem. Soc.* **2015**, *137*, 6492–6495.

(43) Chen, Y.; Tang, Z.; Zhang, X.; Liu, Y.; Wu, S.; Guo, B. Covalently Cross-Linked Elastomers with Self-Healing and Malleable Abilities Enabled by Boronic Ester Bonds. *ACS Appl. Mater. Interfaces* **2018**, *10*, 24224–24231.

(44) Wu, J.; Cai, L.-H.; Weitz, D. A. Tough Self-Healing Elastomers by Molecular Enforced Integration of Covalent and Reversible Networks. *Adv. Mater.* **2017**, *29*, 1702616.

(45) Zhao, L.; Li, X.; Li, Y.; Wang, X.; Yang, W.; Ren, J. Polypyrrole-Doped Conductive Self-Healing Composite Hydrogels with High Toughness and Stretchability. *Biomacromolecules* **2021**, *22*, 1273–1281.

(46) Zhu, Y.; Shen, Q.; Wei, L.; Fu, X.; Huang, C.; Zhu, Y.; Zhao, L.; Huang, G.; Wu, J. Ultra-Tough, Strong, and Defect-Tolerant

Elastomers with Self-Healing and Intelligent-Responsive Abilities. *ACS Appl. Mater. Interfaces* **2019**, *11*, 29373–29381.

(47) Yin, L.-J.; Zhao, Y.; Zhu, J.; Yang, M.; Zhao, H.; Pei, J.-Y.; Zhong, S.-L.; Dang, Z.-M. Soft, tough, and fast polyacrylate dielectric elastomer for non-magnetic motor. *Nat. Commun.* **2021**, *12*, 4517.

(48) Ying, W. B.; Yu, Z.; Kim, D. H.; Lee, K. J.; Hu, H.; Liu, Y.; Kong, Z.; Wang, K.; Shang, J.; Zhang, R.; Zhu, J.; Li, R.-W. Waterproof, Highly Tough, and Fast Self-Healing Polyurethane for Durable Electronic Skin. *ACS Appl. Mater. Interfaces* **2020**, *12*, 11072–11083.

(49) Ying, W. B.; Wang, G.; Kong, Z.; Yao, C. K.; Wang, Y.; Hu, H.; Li, F.; Chen, C.; Tian, Y.; Zhang, J.; Zhang, R.; Zhu, J. A Biologically Muscle-Inspired Polyurethane with Super-Tough, Thermal Repairable and Self-Healing Capabilities for Stretchable Electronics. *Adv. Funct. Mater.* **2021**, *31*, 2009869.

(50) Yao, Y.; Liu, B.; Xu, Z.; Yang, J.; Liu, W. An unparalleled H-bonding and ion-bonding cross-linked waterborne polyurethane with super toughness and unprecedented fracture energy. *Mater. Horiz.* **2021**, *8*, 2742–2749.

(51) Rahman, S. S.; Arshad, M.; Qureshi, A.; Ullah, A. Fabrication of a Self-Healing, 3D Printable, and Reprocessable Biobased Elastomer. *ACS Appl. Mater. Interfaces* **2020**, *12*, 51927–51939.

(52) Li, Y.; Li, W.; Sun, A.; Jing, M.; Liu, X.; Wei, L.; Wu, K.; Fu, Q. A self-reinforcing and self-healing elastomer with high strength, unprecedented toughness and room-temperature reparability. *Mater. Horiz.* **2021**, *8*, 267–275.

(53) Ekeocha, J.; Ellingford, C.; Pan, M.; Wemyss, A. M.; Bowen, C.; Wan, C. Challenges and Opportunities of Self-Healing Polymers and Devices for Extreme and Hostile Environments. *Adv. Mater.* **2021**, *33*, 2008052.

(54) Yu, X.; Zheng, Y.; Wang, Y.; Zhang, H.; Song, H.; Li, Z.; Fan, X.; Liu, T. Facile Fabrication of Highly Stretchable, Stable, and Self-Healing Ion-Conductive Sensors for Monitoring Human Motions. *Chem. Mater.* **2022**, *34*, 1110–1120.

(55) Jiang, N.; Li, H.; Hu, D.; Xu, Y.; Hu, Y.; Zhu, Y.; Han, X.; Zhao, G.; Chen, J.; Chang, X.; Xi, M.; Yuan, Q. Stretchable strain and temperature sensor based on fibrous polyurethane film saturated with ionic liquid. *Compos. Commun.* **2021**, *27*, 100845.

(56) Wang, L.; Ma, J.; Hong, W.; Zhang, H.; Lin, J. Nanoscale Diffusion of Polymer-Grafted Nanoparticles in Entangled Polymer Melts. *Macromolecules* **2020**, *53*, 8393–8399.

(57) Wang, A.; Wang, Y.; Zhang, B.; Wan, K.; Zhu, J.; Xu, J.; Zhang, C.; Liu, T. Hydrogen-bonded network enables semi-interpenetrating ionic conductive hydrogels with high stretchability and excellent fatigue resistance for capacitive/resistive bimodal sensors. *Chem. Eng. J.* **2021**, *411*, 128506.

(58) Wu, Y.; Zeng, Y.; Chen, Y.; Li, C.; Qiu, R.; Liu, W. Photocurable 3D Printing of High Toughness and Self-Healing Hydrogels for Customized Wearable Flexible Sensors. *Adv. Funct. Mater.* **2021**, *31*, 2107202.

(59) Li, R. a.; Fan, T.; Chen, G.; Xie, H.; Su, B.; He, M. Highly transparent, self-healing conductive elastomers enabled by synergistic hydrogen bonding interactions. *Chem. Eng. J.* **2020**, *393*, 124685.

(60) Si, P.; Jiang, F.; Cheng, Q. S.; Rivers, G.; Xie, H.; Kyaw, A. K. K.; Zhao, B. Triple non-covalent dynamic interactions enabled a tough and rapid room temperature self-healing elastomer for next-generation soft antennas. *J. Mater. Chem. A* **2020**, *8*, 25073–25084.

(61) Yang, J.; Wang, T.; Guo, R.; Yao, D.; Guo, W.; Liu, S.; Li, Z.; Wang, Y.; Li, H. Self-Healing Material with Reversible Luminescence Switch Behavior. *ACS Appl. Mater. Interfaces* **2020**, *12*, 54026–54034.

(62) Liu, X.; Chen, X.; Chi, X.; Feng, Z.; Yang, C.; Gao, R.; Li, S.; Zhang, C.; Chen, X.; Huang, P.; Dong, A.; Kong, D.; Wang, W. Biomimetic integration of tough polymer elastomer with conductive hydrogel for highly stretchable, flexible electronic. *Nano Energy* **2022**, *92*, 106735.

(63) O'Connor, K. S.; Watts, A.; Vaidya, T.; LaPointe, A. M.; Hillmyer, M. A.; Coates, G. W. Controlled Chain Walking for the Synthesis of Thermoplastic Polyolefin Elastomers: Synthesis, Structure, and Properties. *Macromolecules* **2016**, *49*, 6743–6751.